Bol. Soc. Paran. Mat.
©SPM – E-ISSN-2175-1188
SPM: www.spm.uem.br/bspm

(3s.) **v. 2026 (44) 4** : 1–27.
ISSN-0037-8712
doi:10.5269/bspm.79930

Numerical Investigation of Porous Parameter Influence on Casson-Type Hybrid Nanofluid ($Ag+TiO_2$ with Base Fluid Blood) Convection with Variable Properties

Annapurna Tarapuram, Syed Mohiuddin, M. Karuna Prasad, Suneetha Kolasani

ABSTRACT: The purpose of the study is to examine the heat and fluid transport properties of a Casson hybrid nanofluid, which is made up of blood and nanoparticles, as it passes down a vertical porous channel while being affected by a magnetic field. Understanding the effects of changing viscosity, variable thermal conductivity, and porous resistance on temperature and velocity distributions pertinent to biological applications, including targeted drug administration, cryosurgery and hyperthermia, is the main goal of the work. **Methodology**: A combination of Casson rheology, viscous dissipation, variable viscosity, variable thermal conductivity and porous resistance effects are used to formulate the governing momentum and energy equations. We use MATLAB's bvp5c solver to numerically solve these nonlinear coupled equations after they have been nondimensionalized. For important dimensionless quantities, such as the Casson parameter, Brinkman number, Hartmann number, wall temperature ratio, and porosity parameter, parametric studies are performed. **Findings:** The findings show that porous resistance alters thermal boundary layers and significantly reduces velocity. When compared to pure blood, the addition of hybrid nanoparticles improves convective heat transmission by as much as 15.80%. While variable thermal conductivity enhances control over heat transfer and steepens temperature gradients, variable viscosity increases flow resistance and decreases peak velocity. **Conclusions:** The study emphasizes how heat and fluid flow behavior in biomedical systems are greatly influenced by the combined impacts of magnetic fields, porous resistance, and thermophysical changes. By separating porosity effects in Casson hybrid nanofluid flow without the contribution of an electric field, the novelty offers practical information about heat transport aided by nanoparticles in porous biological tissues and manufactured scaffolds.

Keywords: Casson hybrid nanofluid, porous medium, viscous dissipation, MHD, variable viscosity, variable thermal conductivity.

Contents

1 Introduction **1**

2 Mathematical Formulation **4**
2.1 The surface skin friction and Nusselt number: 6

3 Solution Methodology **7**

4 Results and Discussion **8**

5 Skin Friction and Nusselt Number Analysis **20**

6 Comparison of Numerical Solutions for Velocity and Temperature **22**

7 Conclusion **23**

1. Introduction

The ability of the hybrid nanofluids to increase heat transfer in a way that is not possible with the traditional single-phase fluids has drawn a significant amount of interest. They are produced by the dispersion of various types of nanoparticles in a base fluid, giving them better thermal characteristics, such as higher thermal conductivity and better convective heat transfer, than fluids with one type of nanoparticle. Therefore, hybrid nanofluids have a great potential in advanced thermal management in engineering, energy and biomedical fields. The first to suggest the idea of dispersing nanoparticles in pure fluids to enhance thermal performance was [1], [2] studied the influences of hydrothermal changes

2020 *Mathematics Subject Classification:* 76Z05.
Submitted November 11, 2025. Published February 26, 2026

on radiative nanofluid flow, including the presence of nanolayers and nanoparticle diameter. The current research is on a Casson-type hybrid nanofluid that is composed of silver (Ag) and titanium dioxide (TiO_2) nanoparticles suspended in blood, which is the base fluid. Blood is a non-Newtonian fluid with a complex shear-thinning property i.e., the viscosity of blood reduces with the shear rate. This factor renders it hard to understand the heat conduction and fluid mechanics in these systems. In addition, non-Newtonian properties of blood, hybrid nanoparticles, and complex convectional patterns in porous media ought to be carefully analyzed throughout the process of modeling and optimization of real-life applications [3], [4], [5] and [6]. The suspension of red blood cells in the plasma causes the non-Newtonian characteristics of blood. According to [7] composite nanoparticles were detected in the blood circulation of the arteries, and this led to a tremendous desire to develop non-Newtonian fluid models, including the Casson fluid model. The model is used to improve the knowledge of the mechanics of blood flow in the circulatory system and helps in the investigation of cardiovascular pathologies [8], [9], [10], [11] and [12]. The Casson fluid model plays a role in the description of the complicated rheological properties of bio fluids such as blood that are likely to have shear-thinning properties. The model is vital in the dynamics of physiological flows because it can be applied in the explanation of the special viscoelastic properties of such fluids at different shear rates. Moreover, it is necessary to take into account the variable nature of the base fluid (blood) and the porous medium to have a realistic modeling of the system. Viscosity and thermal conductivity of blood may also be dependent on temperature, shear rates, and a thorough investigation regarding these aspects and their relation to heat transfer and fluid flow is required. The porous structure that contains the flowing fluid is also a significant issue of the hybrid nanofluid's overall performance, since the interactions between the fluid and the porous structure have a great influence on the heat transport processes. The flow of porous media is an essential part in many applications in heat transfer like biomedical devices, geothermal reservoirs and heat exchangers [13], [14] and [15]. The porous media also adds extra resistance to the flow of fluids and this affects the velocity field, temperature field, and the rate of heat transfer in the system. This interface between the porous matrix and the nanofluid is important in increasing or limiting thermal movement [16] explored the study of the change in thermal conductivity of the magneto-hybrid nanofluids flow through a porous medium with variable viscosity and slip boundary. The overall heat convection performance of the porous medium is heavily impacted by the permeability and porosity of the porous medium, coupled with the thermal conductivity of the porous structure, and also the thermal conductivity of the nanofluid. The subsequent researchers, suchstems, which have fixed fluid properties, yet the effect of hybrid nanoparticles (Ag and TiO_2) in a Casson-type flu as [17], [18] and [19] are still carrying out further research on the effects of thermal radiation, thermal conductivity, and variable viscosity under the porous medium. In addition to this, the time varying viscosity and thermal conductivity of the hybrid nanofluid to changes in temperature and shear rate are also a variable that makes the analysis a complex one. The viscosity of blood, which can be affected by such variables as shear rate and temperature, and the non-Newtonian character of Casson fluid, provides essential deviation in the flow and heat transfer behavior [20], [21], [22], [23], [24] and [25]. Therefore, these nonlinear temperature dependent properties are to be properly accounted for in accurate numerical models in order to realistically model the performance of the system. Cross relation of nanofluids, convective heat transfer, and porous media with changing thermal and flow characteristics is an ambiguous and developing field of study. Existing literature has concentrated on single component nanofluids or idealized syid, when the properties of the porous medium are temperature dependent, has not been adequately investigated. These factors, combined with the even more complex variable viscosity and thermal conductivity, are one of the major gaps in the existing research. Although hybrid nanofluids have good prospects, there are a number of challenges that have to be overcome in this study. The former is the simultaneous assessment of the changes in viscosity and conductivity at physiological conditions. The second one is a holistic numeric treatment that connects the biomedical transport phenomena to energy engineering. The third is the discussion of the porosity effects in a realistic and non Newtonian fluid system (blood), which is not extensive in the current literature.

Objectives:
The proposed research will analyze the influence of parameters of porous media on the nature of convective heat transfer of a Casson type hybrid nanofluid (Ag + TiO_2 in blood) with varying viscosity and

thermal conductivity. Specifically, the objectives are the following.

- To Ascertain the effect of porosity, permeability and other properties of porous media on the heat transfer and fluid flow properties.
- To model the temperature and shear rate dependence of viscosity and thermal conductivity of the hybrid nanofluid.
- To quantify the heat transfer enhancement provided by hybrid nanoparticles ($Ag + TiO_2$) in normal physiological conditions in blood.

Application:
The present study has immense implications for numerous aspects of practice: [26]

- Cancer therapy and focused drug delivery in which an accurate manipulation of thermo-relaxation is essential.
- Blood perfusion and artificial organs with improved transportation of heat to simulate physiological conditions.
- Nanoparticles show potential for antimicrobial applications and targeted drug delivery, but there are significant biological and safety concerns, including the toxicity of silver nanoparticles,immune system interactions, bioaccumulation and blood compatibility. These factors must be thoroughly evaluated before clinical use. While ongoing research suggests that with proper modifications, these nanoparticles could be more biocompatible, their safety and efficacy for blood circulation require extensive testing before medical application [27], [28].
- High-end heat exchangers and cooling gadgets require flexible thermal conductivity and viscosity. Modelling external heating and cooling in Casson hybrid nanofluids is significant for biomedical and engineering applications. In medicine, enhanced thermal conductivity enables precise temperature control for hyperthermia and targeted drug delivery, improving treatment efficacy. In engineering, such control aids efficient thermal management in biomedical devices like microfluidic systems and artificial organs. The superior thermophysical properties of A nanoparticles ensure improved convective heat transfer and stable operation [29], [30].

Limitations: Even though hybrid nanofluids have great potential, several limitations should be considered: Concurrent analysis of the changes in viscosity and conductivity in the physiological conditions.Macroscopic numerical modelling between biomedical transport phenomena and energy engineering.Handling the porosity effects in a realistic, non-Newtonian fluid system with a blood-based fluid system, also well represented in the literature.

Novelty of the Work: The uniqueness of the present research lies in the combination of the consideration of multiple complicated factors:Concurrent monitoring of the change of viscosity and conductivity at physiological conditions.A holistic numerical solution between biomedical transport physics and energy engineering.Filling the gap in the existing literature by considering the porosity effects in a realistic,non-Newtonian, blood-based fluid system.

2. Mathematical Formulation

In a porous medium, a Casson hybrid nanofluid consisting of blood-mixed silver and titanium dioxide nanoparticles demonstrates both movement and heat transmission properties along with an applied magnetic field as it moves down a vertical tube. A theoretical illustration of the hybrid nanofluid synthesis and preparation process is provided in the figure. 1.

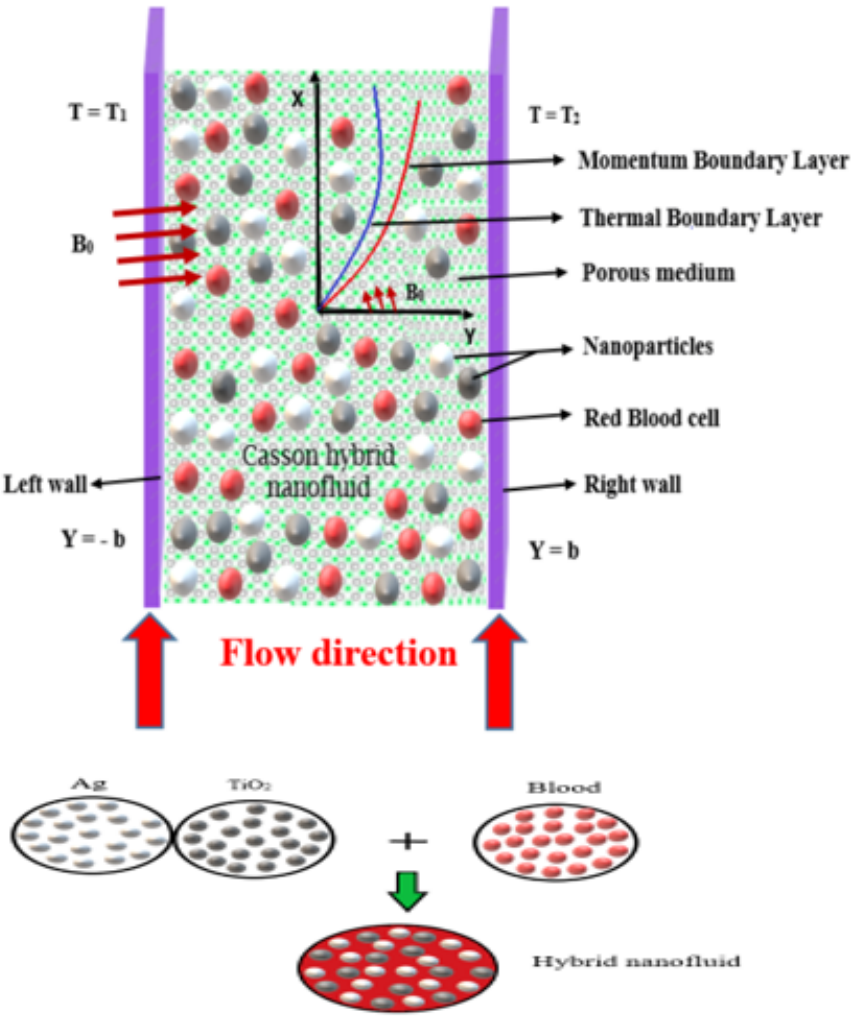

Figure 1: Physical configuration

Preliminary assumptions regarding the issue:

- Figure 1 shows a vertical channel with porous medium fully developed non-Newtonian fluid flow, where the walls are kept at a constant temperature T_1 and T_2 .
- The coordinates $-b \leq Y \leq b$ define the area of interest. Specifically, fluid flow is determined by buoyancy force.
- The rigid walls are unlimited in the X-direction and have zero velocity.

- The character says the situation is essentially one-dimensional. The Boussinesq approximation is valid and the fluids are heat-conducting and viscous.
- When modeling the fluid and heat transmission, the temperature-dependent viscosity and thermal conductivity are taken into account.

The transverse magnetic field, applied inertia, viscous dissipation, and heating can all be used to characterize the governing equations for flexible physical components. Furthermore, the definition of changeable physical attributes is as follows:

$$\left(1+\frac{1}{\lambda_1}\right)\frac{d}{dY}\left(\mu_{hnf}\frac{dq_1}{dY}\right)+(\rho\beta)_{hnf}g(T-T_0)-\frac{\mu_{hnf}}{\kappa_1}q_1-\frac{c_f\rho_{hnf}}{\sqrt{\kappa_1}}q_1^2-\sigma_{hnf}B_0^2q_1-\frac{\partial p}{\partial x}=0 \tag{2.1}$$

$$\frac{d}{dY}\left(k_{hnf}\frac{dT}{dY}\right)+\left(1+\frac{1}{\lambda_1}\right)\mu_{hnf}\left(\frac{dq_1}{dY}\right)^2+\frac{\mu_{hnf}}{\kappa_1}q_1^2+\sigma_{hnf}B_0^2q_1^2=0 \tag{2.2}$$

The velocity and temperature field's boundary conditions are

$$q_1=0 \quad \text{at} \quad Y=\pm b \tag{2.3}$$

$$T=T_1 \quad \text{at} \quad Y=-b, \quad \text{and} \quad T=T_2 \quad \text{at} \quad Y=b \tag{2.4}$$

The fundamental thermophysical characteristics of the Hybrid nanofluid are [31], [32]

$$\frac{\mu_{hnf}}{\mu_f}=\left[\frac{1}{(1-\phi_{TiO_2})^{2.5}(1-\phi_{Ag})^{2.5}}\right],$$

$$\frac{k_{hnf}}{k_{nf}}=\left[\frac{k_{Ag}+2k_{nf}-2\phi_{Ag}(k_{nf}-k_{Ag})}{k_{Ag}+2k_{nf}+\phi_{Ag}(k_f-k_{Ag})}\right],$$

where

$$\frac{k_{nf}}{k_f}=\left[\frac{k_{TiO_2}+2k_f-2\phi_{TiO_2}(k_f-k_{TiO_2})}{k_{TiO_2}+2k_f+\phi_{TiO_2}(k_f-k_{TiO_2})}\right]$$

$$\left(\frac{(\rho\beta)_{hnf}}{(\rho\beta)_f}\right)=\left[(1-\phi_{Ag})\left((1-\phi_{TiO_2})+\phi_{TiO_2}\frac{\rho_{TiO_2}\beta_{TiO_2}}{\rho_f\beta_f}\right)+\phi_{Ag}\frac{\rho_{Ag}\beta_{Ag}}{\rho_f\beta_f}\right],$$

$$\frac{\sigma_{hnf}}{\sigma_{nf}}=\left[\frac{\sigma_{Ag}+2\sigma_{nf}-2\phi_{Ag}(\sigma_{nf}-\sigma_{Ag})}{\sigma_{Ag}+2\sigma_{nf}+\phi_{Ag}(\sigma_{nf}-\sigma_{Ag})}\right],$$

where

$$\frac{\sigma_{nf}}{\sigma_f}=[\frac{\sigma_{TiO_2}+2\sigma_f-2\phi_{TiO_2}(\sigma_f-\sigma_{TiO_2})}{\sigma_{TiO_2}+2\sigma_f+\phi_{TiO_2}(\sigma_f-\sigma_{TiO_2})}],$$

$$\frac{\rho_{hnf}}{\rho_f}=\left[(1-\phi_{Ag})\left((1-\phi_{TiO_2})+\phi_{TiO_2}\frac{\rho_{TiO_2}}{\rho_f}\right)+\phi_{Ag}\frac{\rho_{Ag}}{\rho_f}\right],$$

where

$$\begin{aligned}
&C_1=\frac{\mu_{hnf}}{\mu_f}, \quad C_2=\frac{k_{nf}}{k_f}, \quad C_3=\frac{k_{hnf}}{k_{nf}}, \quad C_4=C_3\times C_2,\\
&C_5=\left(\frac{(\rho\beta)_{hnf}}{(\rho\beta)_f}\right), \quad C_6=\frac{\sigma_{nf}}{\sigma_f}, \quad C_7=\frac{\sigma_{hnf}}{\sigma_{nf}}, \quad C_8=C_7\times C_6,\\
&C_9=\frac{\rho_{hnf}}{\rho_{nf}}
\end{aligned} \tag{2.5}$$

The fluid viscosity $'\mu'$ is considered as follows [33], [34]

$$\mu=\mu_0 e^{-b(T-T_0)} \tag{2.6}$$

where $'b'$ is an empirical constant.

The fluid's thermal conductivity is considered to be [33], [34]

$$K = K_0 e^{-b(T-T_0)} = K_0\big(1 + b(T_0 - T)\big) \tag{2.7}$$

Equations (1) and (2) can be written in a non-dimensional form using the following parameters [35], [36]

$$q = \frac{q_1}{\bar{q}}, \quad y = \frac{Y}{b}, \quad n = \frac{T_1 - T_2}{\Delta T}, \quad \theta = \frac{T - T_0}{\Delta T}, \quad P = \frac{b^2}{\mu_0 \bar{q}}\frac{\partial p}{\partial x}, \quad Br = \frac{\mu_0 q_r^2}{k_0 \Delta T}, \quad Re = \frac{\bar{q} b}{\gamma_f},$$

$$\gamma_f = \frac{\mu_f}{\rho_f}, \quad \sigma = \frac{b}{\sqrt{k_1}}, Gr = \frac{g\beta_f b^3 \Delta T}{\gamma_f^2}, \quad Gr = \frac{Gr}{Re}, \quad M^2 = \frac{\sigma_f B_0^2 b^2}{\mu_f}, \quad \sigma = \frac{\rho_f c_f \bar{q} b^2}{\sqrt{k_f}\mu_f} \tag{2.8}$$

Using temperature dependence for velocity (5) and thermal conductivity (6)the governing equation (1) to (4) can be reduced to:

$$\frac{d^2 q}{dy^2} - u_v \frac{d\theta}{dy}\frac{dq}{dy} + d_6 Gr_{t_1}\left(1 + u_v\theta\right)\theta - d_1\sigma^2 q - d_7\delta q^2 - d_8 M^2 q - d_5\left(1 + u_v\theta\right)P = 0 \tag{2.9}$$

$$\frac{d^2 q}{dy^2} - u_k\left(\frac{d\theta}{dy}\right)^2 + d_{11}Br\left(\frac{dq}{dy}\right)^2 + d_{11}Br(u_k - u_r)\theta\left(\frac{dq}{dy}\right)^2 - d_{11}Bru_k u_v\theta^2\left(\frac{dq}{dy}\right)^2 + d_9 Br\sigma^2 q^2$$

$$+d_9 Br\sigma^2(u_k - u_v)\theta^2 q^2 - d_9 Br\sigma^2 u_v u_k \theta^2 q^2 + d_{10}BrM^2\left(1 - u_v\theta\right)\left(1 + u_k\theta\right)q^2 = 0 \tag{2.10}$$

where,

$$u_v = b\Delta T, \quad u_k = b\Delta T, \quad d_1 = \frac{1}{\left(1 + \frac{1}{\lambda_1}\right)}, \quad d_2 = \frac{C_5}{C_1}, \quad d_3 = \frac{C_9}{C_1}, \quad d_4 = \frac{C_8}{C_1}, \quad d_5 = \frac{d_1}{C_1},$$

$$d_6 = d_1 \times d_2, \quad d_7 = d_1 \times d_3, \quad d_8 = d_1 \times d_4, \quad d_9 = \frac{C_1}{C_4}, \quad d_{10} = \frac{C_8}{C_4}, \quad d_{11} = \frac{d_9}{d_1} \tag{2.11}$$

2.1. The surface skin friction and Nusselt number:

During the current problem we also defined the following parameters: the dimensionless skin friction

$$\tau_1 = e^{u_v}(1 + n)\left(\frac{dq}{dy}\right)_{y=-1}, \qquad \tau_2 = e^{u_v}\left(\frac{dq}{dy}\right)_{y=1} \tag{2.12}$$

The dimensionless form becomes

$$Nu = \frac{d\left(K\,\frac{dT}{dy}\right)_{y=\pm b}}{K_0\,\Delta T} \tag{2.13}$$

$$Nu_1 = -(1 + u_v(1 + n))\left(\frac{d\theta}{dy}\right)_{y=-1}, \quad \text{and} \quad Nu_2 = -(1 + u_v)\left(\frac{dq}{dy}\right)_{y=1} \tag{2.14}$$

The boundary conditions in the non-dimensional form are written as follows:

$$q = 0 \quad \text{at} \quad y = \pm 1$$

$$\theta = 1 + n \quad \text{at} \quad y = -1, \qquad \theta = 1 \quad \text{at} \quad y = 1 \tag{2.15}$$

3. Solution Methodology

The Bvp5c solver in MATLAB is used to obtain numerical solutions. A numerical technique called BVP5C is used to tackle boundary value issues for differential equation systems that are extremely non-linear. BVP5C is a MATLAB solver for Boundary Value Problems (BVPs) with unknown parameters. The BVP5C flow chart is described.

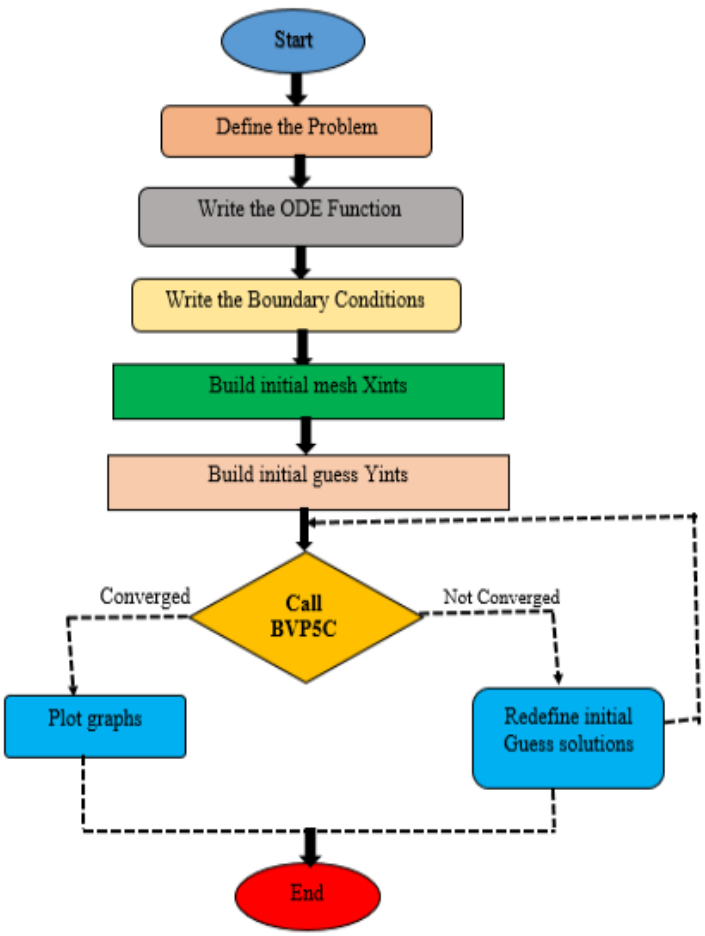

Figure 2: Flow Chart

Table 1: Lists baseline thermophysical properties for the base fluid and the two constituent nanoparticles [37], [38].

Physical feature	Blood	Ag	TiO_2
ρ (kg/m^3)	1050	10500	4250
k (W/m·K)	0.52	429	8.9538
β_t (K^{-1})	0.18×10^{-2}	1.89×10^{-5}	0.9×10^{-5}
σ (S/m)	6.67×10^{-1}	6.3×10^{7}	2.38×10^{4}
μ (Pa.s)	3.5×10^{-3} - 5.5×10^{-3}	0.01	0.01

4. Results and Discussion

This section presents a detailed analysis of the velocity and temperature variations for Casson hybrid nanofluid flow through a porous channel under different physical effects. Figures 3 to 24 depict how parameters such as variable viscosity u_v and thermal conductivity u_k, thermal Grashof number Gr_{t_1}, Brinkman number Br, wall temperature ratio n, porous resistance σ_1, Casson parameter λ_1, nanoparticle volume fractions ϕ_1, ϕ_2, Hartmann number M and inertia parameter δ influence momentum and thermal boundary layers. Each explanation discusses the nature of the profile, the reason for its behavior and its physical implications Figure 3 shows that the velocity profile increases as the variable viscosity parameter u_v increases. A larger reduces the effective viscosity of the fluid, lowering internal resistance and momentum diffusion. With reduced viscous drag, the fluid accelerates more easily, resulting in higher velocity values across the domain. Consequently, the hydrodynamic boundary layer becomes thicker and the overall flow strength is enhanced compared to the constant viscosity case. Figure 4 indicates that temperature rises as the variable viscosity parameter u_v increases. Enhanced viscosity reduces fluid motion, leading to higher viscous dissipation and heat retention within the fluid. This retained thermal energy causes the thermal boundary layer to expand. As a result observed by [39] temperature gradients weaken and temperature distribution becomes more uniform. Figure 5 demonstrates that velocity decreases as the variable thermal conductivity parameter u_k increases. Increased conductivity accelerates heat diffusion, which weakens buoyancy forces and diminishes fluid acceleration. Consequently, momentum transfer slows and the hydrodynamic boundary layer becomes thinner. The overall velocity field shows a significant reduction compared to low conductivity cases. Figure 6 reveals that temperature decreases with higher thermal conductivity u_k. Enhanced conduction facilitates rapid heat dispersion, reducing local temperature gradients and limiting temperature rise within the fluid. This results in a thinner thermal boundary layer and lower surface temperature. Thermal diffusion dominates over convective effects in this regime. Figure 7 shows that velocity increases with the thermal Grashof number Gr_{t_1}. A higher Grashof number Gr_{t_1} reflects stronger buoyancy forces generated by temperature differences, which assist in driving the flow. Enhanced buoyancy overcomes viscous resistance and accelerates the fluid motion. This leads to a thicker velocity boundary layer and higher flow rates near the centerline. Figure 8 illustrates that temperature increases as the thermal Grashof number Gr_{t_1} increases. Buoyancy induced convection strengthens heat transport, carrying more thermal energy into the fluid domain. This expansion of the thermal boundary layer raises the overall temperature distribution. As a result, convective effects dominate over conduction at higher Grashof numbers Gr_{t_1}, Figure 9 shows that velocity increases with Brinkman number Br. A higher Brinkman number Br indicates increased viscous dissipation, which contributes additional energy to the fluid and enhances buoyancy driven motion. This increased thermal energy results in greater flow acceleration. Consequently, the velocity profile rises and the hydrodynamic boundary layer expands. Figure 10 demonstrates that temperature increases as Brinkman number Br rises. Viscous heating elevates the thermal energy of the fluid,causing a significant temperature rise across the boundary layer. Enhanced internal heat generation thickens the thermal layer and increases surface temperature. This indicates that viscous effects strongly influence thermal transport at higher Brinkman numbers Br. Figure 11 shows that velocity increases with wall temperature ratio n. A larger temperature difference between the channel walls intensifies buoyancy forces and accelerates fluid motion. The enhanced driving force expands the hydrodynamic boundary layer and elevates peak velocity. Stronger natural convection effects dominate the flow behavior in this condition. Figure 12 reveals that temperature increases with wall temperature ratio n. A steeper temperature gradient enhances convective heat transfer and increases thermal energy within the fluid. The thicker thermal boundary layer results n difference increases. Figure 13 shows that velocity decreases with porous parameter σ_1. Higher porous resistance introduces additional drag, reducing fluid momentum and weakening convective transport. This increased resistance suppresses velocity and thins the boundary layer. Flow resistance from the porous medium dominates over driving forces in this regime. Figure 14 indicates a slight temperature decrease with increasing porous parameter σ_1. Increased drag reduces convective transport efficiency and weakens thermal energy distribution. As a result, the thermal boundary layer becomes thinner and temperature gradients decrease. Heat transfer is primarily controlled by conduction rather than convection here. Figure 15 shows that velocity increases with Casson parameter λ_1. A higher Casson parameter λ_1 indicates reduced yield stress and lower apparent viscosity, allowing fluid motion to accelerate more easily. The

decreased resistance enhances momentum transfer and thickens the hydrodynamic boundary layer. As a result, velocity rises throughout the flow domain. Figure 16 demonstrates that temperature increases as Casson parameter λ_1 increases. Reduced viscous resistance enhances viscous dissipation and thermal energy retention, leading to a thicker thermal boundary layer. Increased thermal diffusion elevates the overall temperature distribution. This effect highlights the role of non-Newtonian rheology in heat transfer processes. Figure 17 Shows that the velocity profile increases with increasing nanoparticle volume fraction ϕ_1. The addition of nanoparticles significantly enhances the effective thermal conductivity and momentum transfer capability of the hybrid nanofluid, which reduces viscous resistance in the flow. This improved momentum transport accelerates the fluid motion, leading to higher velocity throughout the channel. As a result, the hydrodynamic boundary layer becomes thicker, and the effect is more noticeable at higher nanoparticle concentrations. Figure 18 illustrates that temperature increases with nanoparticle volume fraction ϕ_1. Enhanced effective thermal conductivity due to nanoparticles promotes better heat transfer throughout the fluid. This leads to a higher temperature distribution and a thicker thermal boundary layer. Improved energy transport enhances the overall heat transfer performance. Figure 19 shows that the velocity profile increases with an increase in nanoparticle volume fraction ϕ_2. The presence of additional nanoparticles improves the effective thermal and momentum transport properties of the hybrid nanofluid, which reduces viscous resistance and enhances flow acceleration. This improvement in momentum transfer leads to higher velocity values and a thicker hydrodynamic boundary layer. The influence of becomes more significant at higher particle concentrations, where enhanced flow behavior is clearly observed. Figure 20 shows that temperature increases with nanoparticle volume fraction ϕ_2. Improved thermal conductivity facilitates faster heat transport, raising temperature levels and expanding the thermal boundary layer. This enhances overall heat transfer capacity. Higher nanoparticle loading contributes significantly to improved thermal performance. Figure 21 shows that velocity decreases with increasing Hartmann number M. The Lorentz force generated by the applied magnetic field opposes fluid motion, introducing magnetic damping. This reduces flow acceleration and momentum transfer. The velocity boundary layer becomes thinner as electromagnetic effects dominate the flow behavior. Figure 22 shows that the temperature profile decreases with increasing Hartmann number M. A stronger magnetic field introduces a Lorentz force that suppresses fluid motion and reduces kinetic energy within the flow. This magnetic damping effect diminishes convective transport of heat, leading to lower temperature levels throughout the channel. Figure 23 shows that the velocity profile decreases as the inertia parameter δ increases. A higher inertia parameter δ introduces greater inertial resistance, which counteracts the driving forces responsible for fluid motion. This resistance suppresses the flow acceleration and reduces the overall velocity distribution. As a result, the hydrodynamic boundary layer becomes thinner and the fluid motion weakens with increasing δ. Figure 23 shows that the temperature profile decreases with increasing inertia parameter δ. As δ increases, the intensified inertial forces reduce the residence time of fluid particles, which weakens heat absorption and convective heat transport. This leads to a decline in the overall temperature distribution and a thinner thermal boundary layer. Consequently, heat transfer effectiveness decreases as inertia δ becomes more dominant in the flow dynamics.

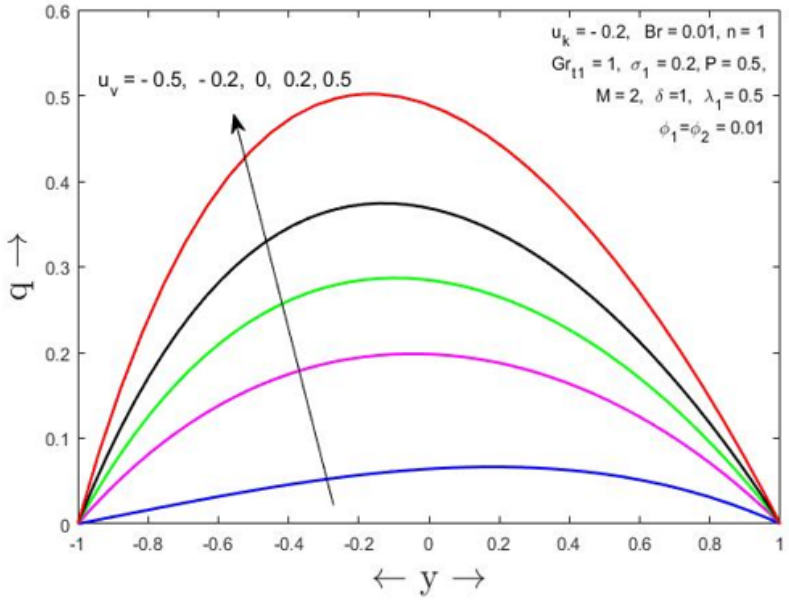

Figure 3: Velocity profiles for various values of u_v

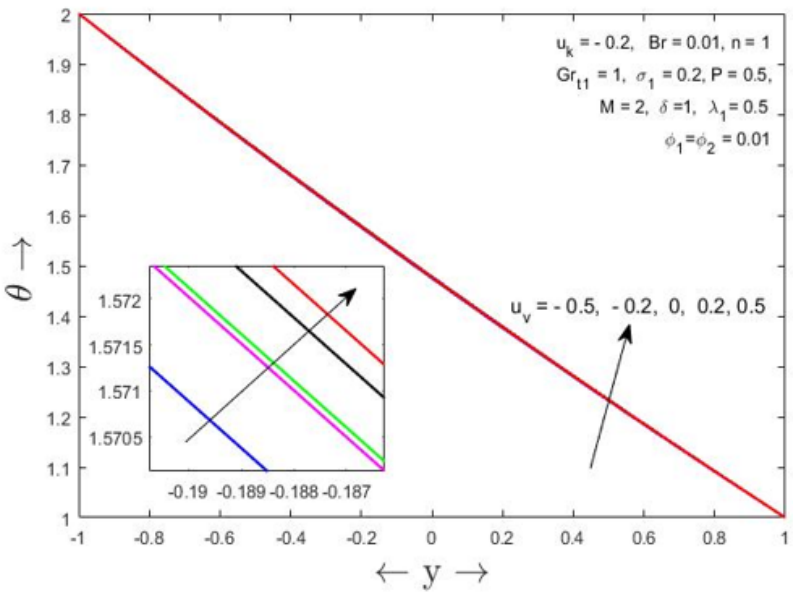

Figure 4: Temperature profiles for various values u_v

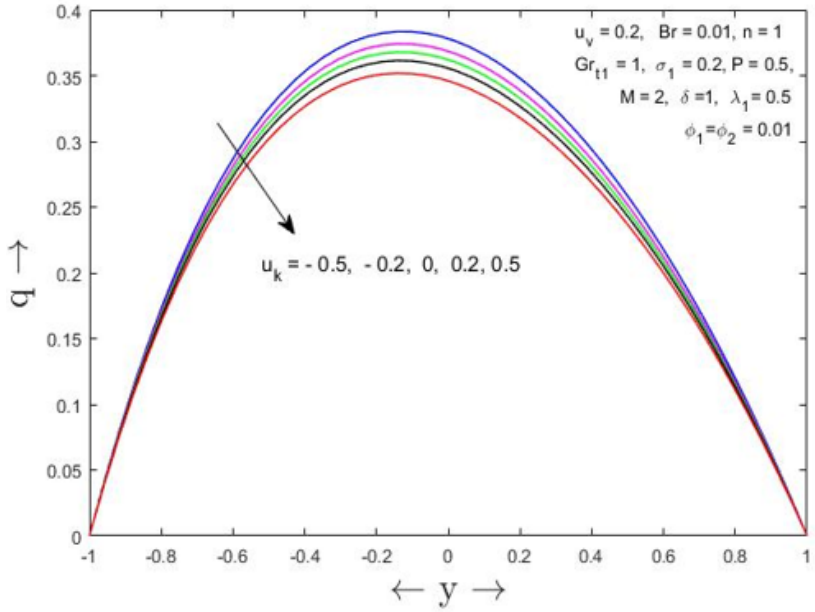

Figure 5: velocity profiles for various values of u_k

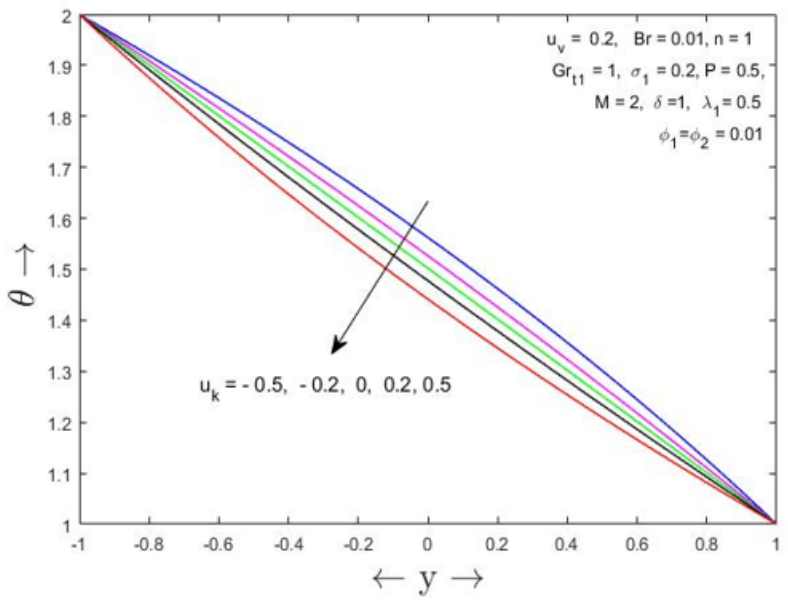

Figure 6: Temperature profiles for various values of u_k

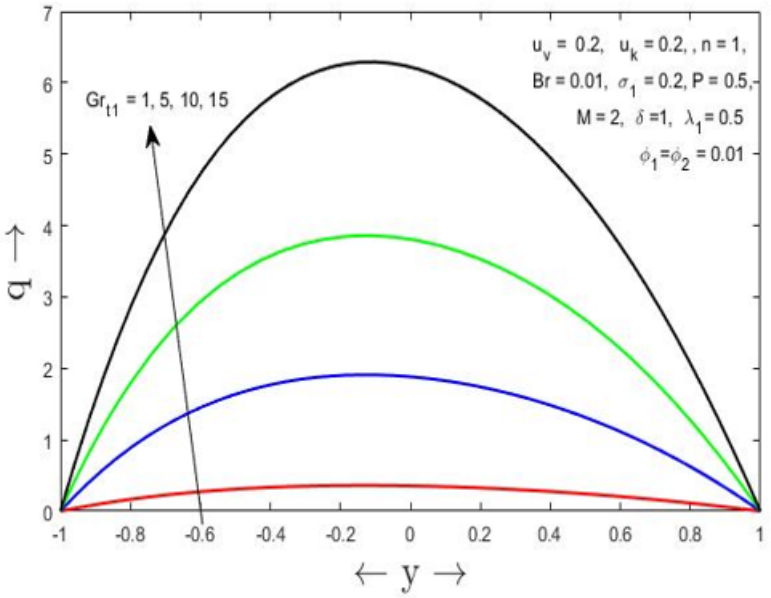

Figure 7: velocity profiles for various values of Gr_{t1}

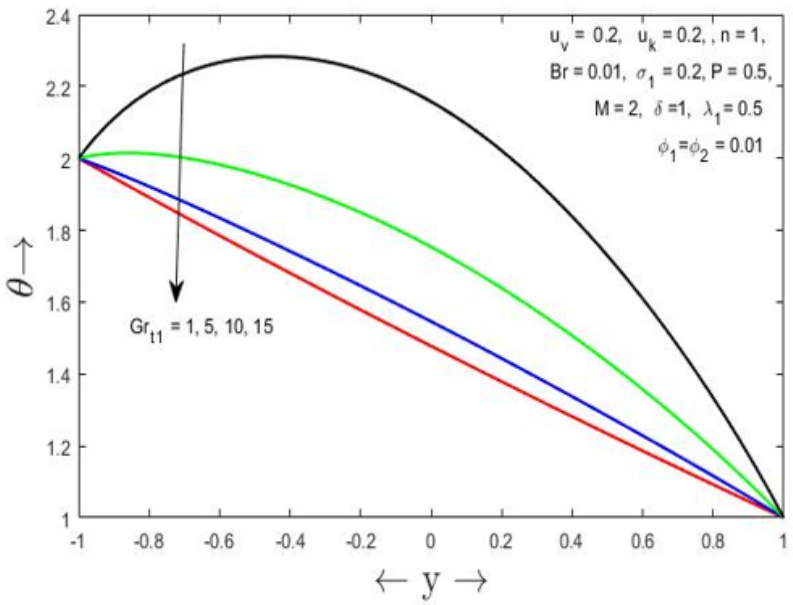

Figure 8: Temperature profiles for various values of Gr_{t_1}

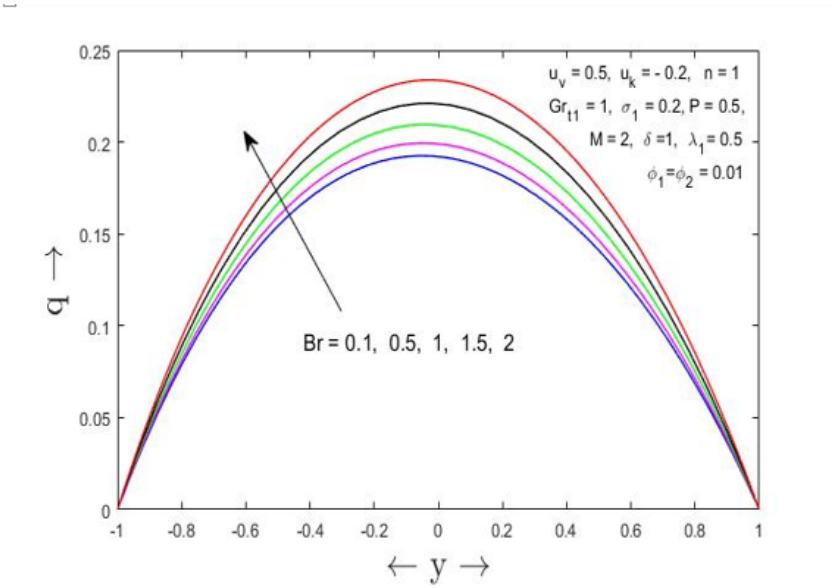

Figure 9: velocity profiles for various values of Br

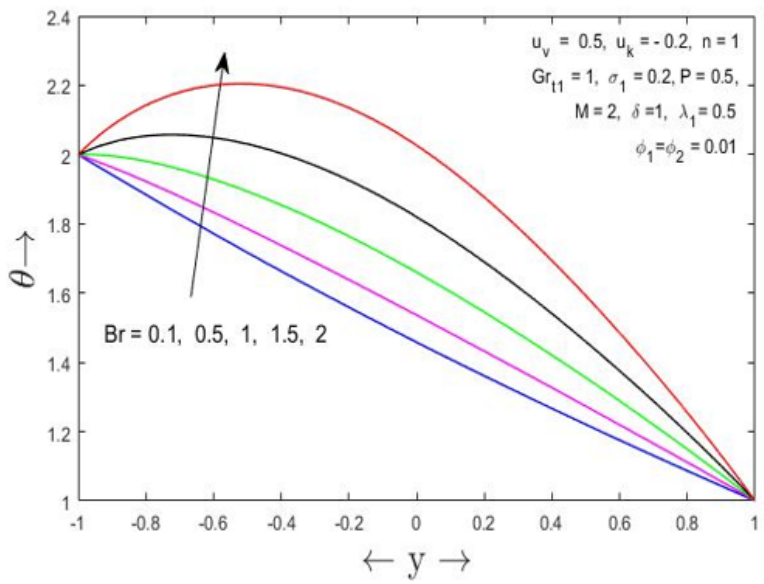

Figure 10: Temperature profiles for various values of Br

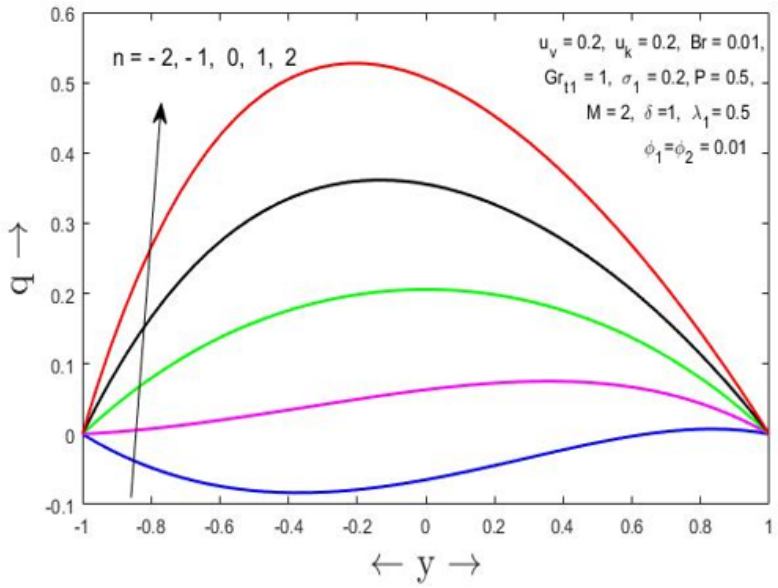

Figure 11: velocity profiles for various values of n

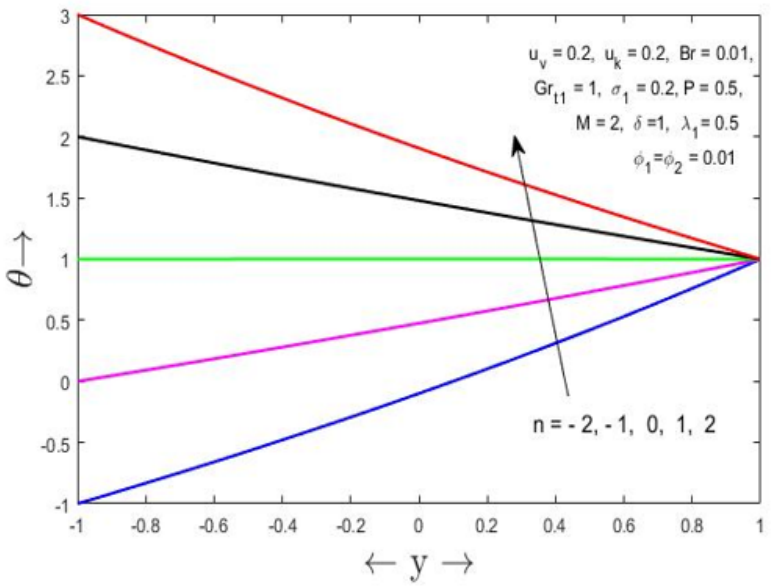

Figure 12: Temperature profiles for various values n

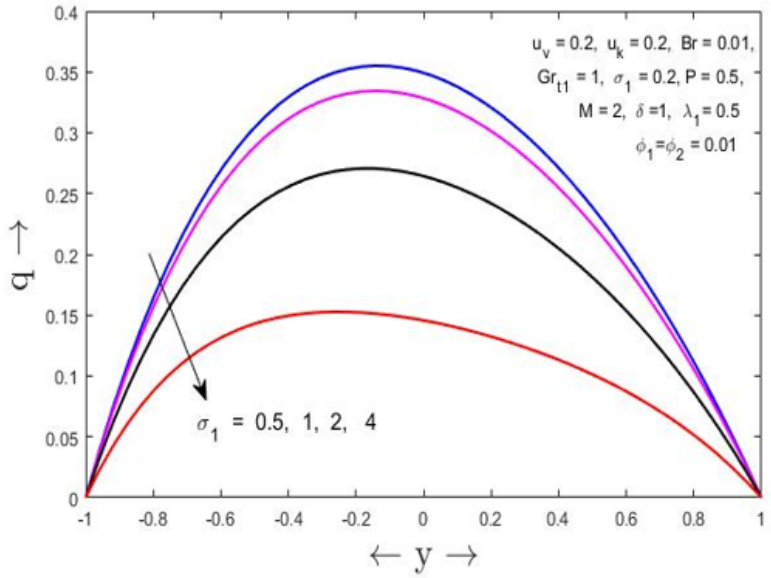

Figure 13: velocity profiles for various values of σ_1

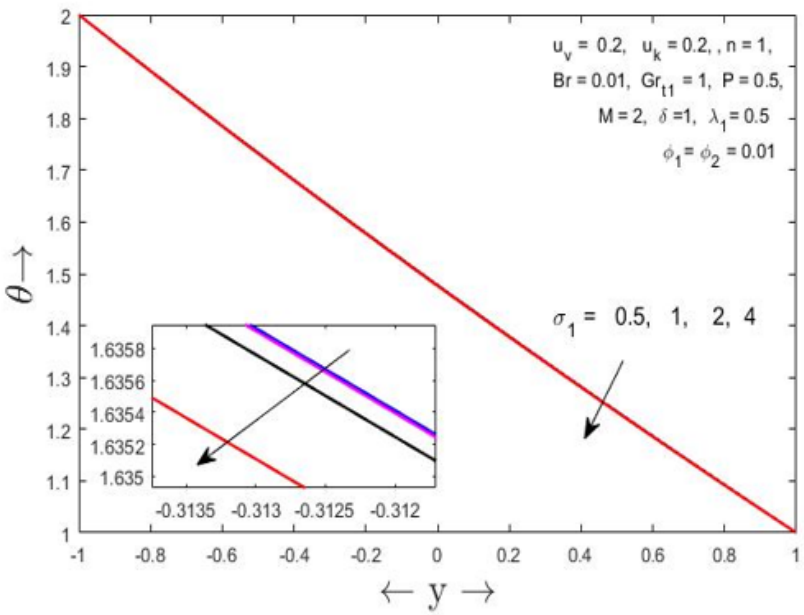

Figure 14: Temperature profiles for various values of σ_1

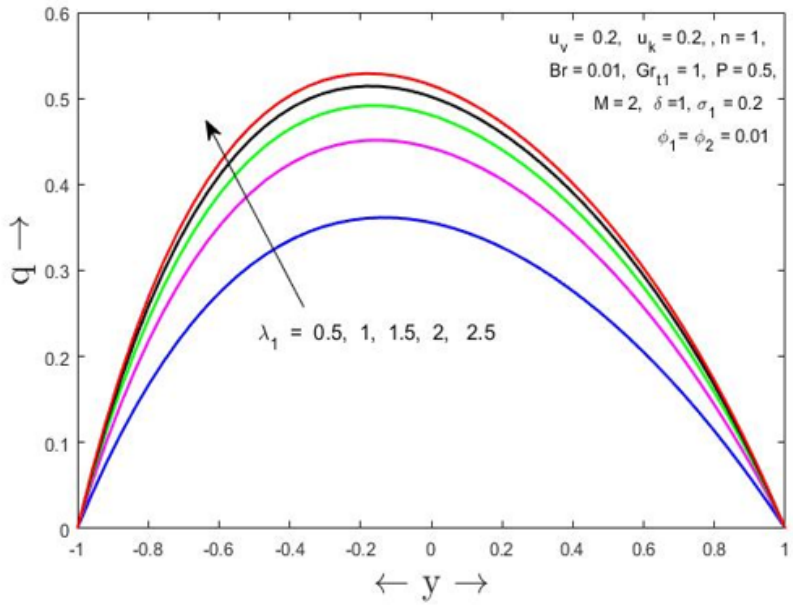

Figure 15: velocity profiles for various values of λ_1

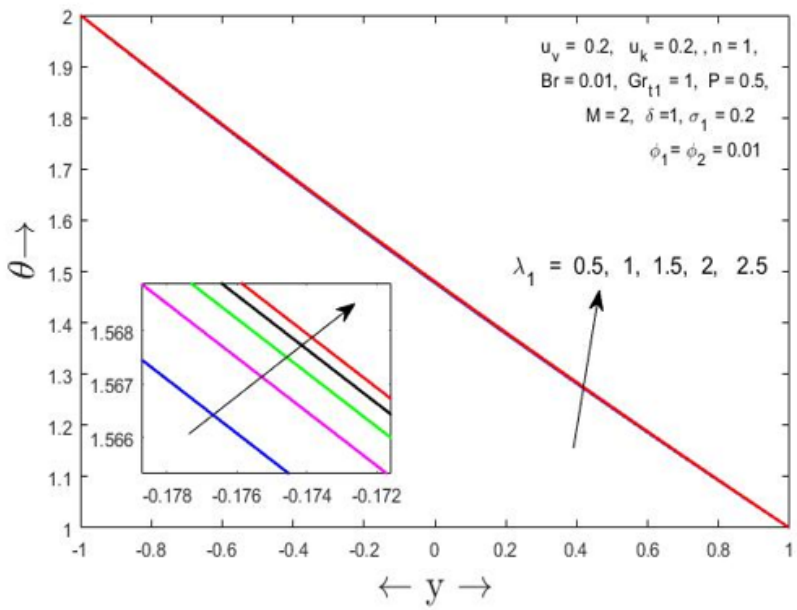

Figure 16: Temperature profiles for various values of λ_1

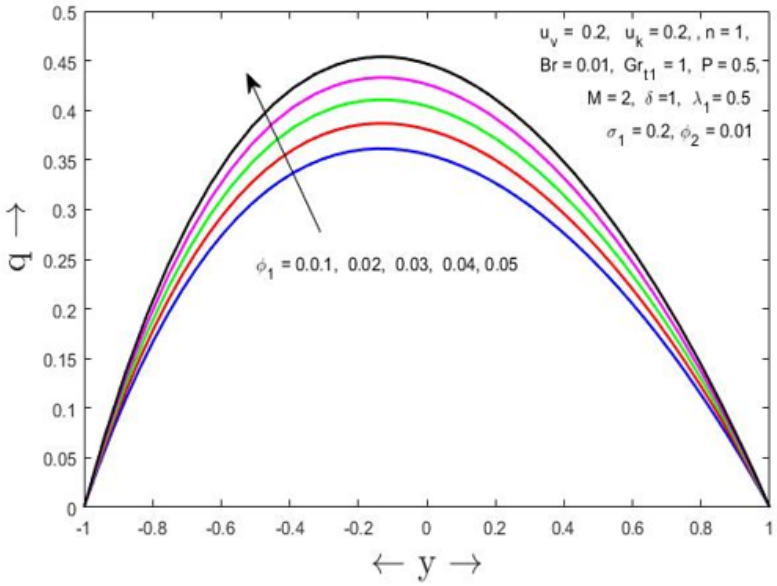

Figure 17: velocity profiles for various values of ϕ_1

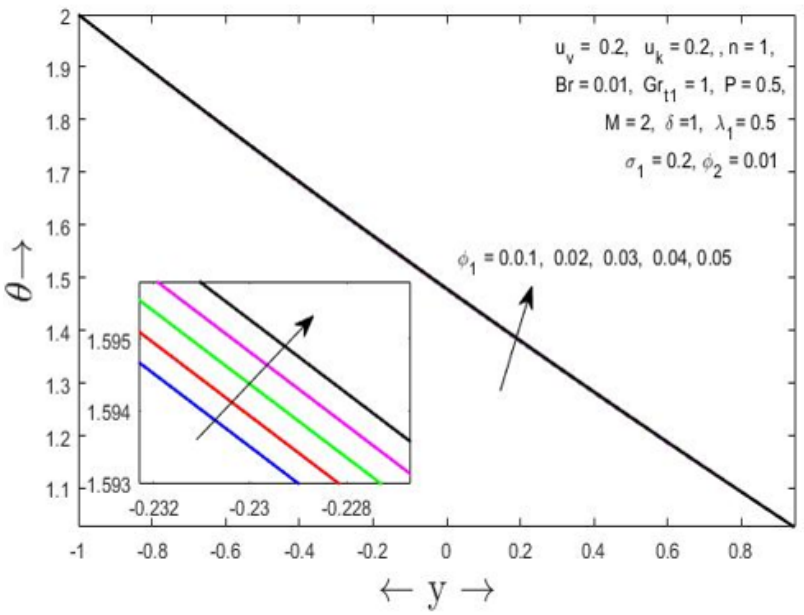

Figure 18: Temperature profiles for various values of ϕ_1

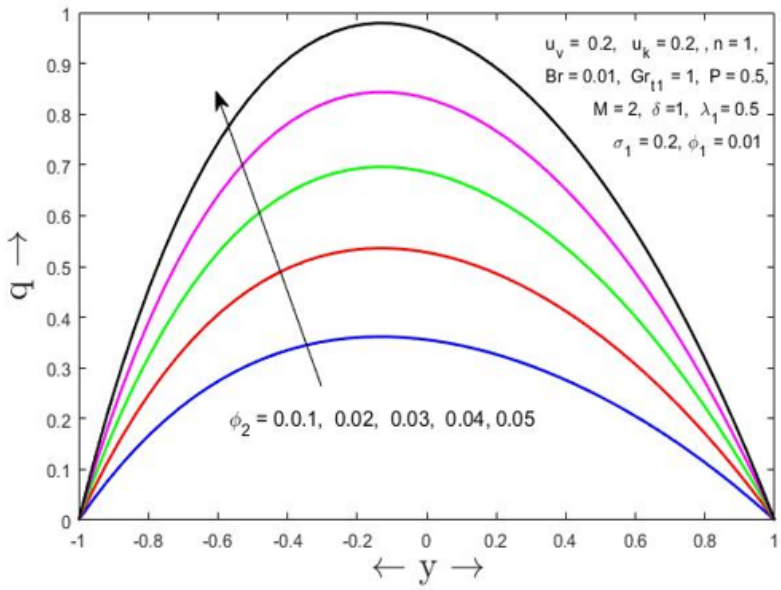

Figure 19: velocity profiles for various values of ϕ_2

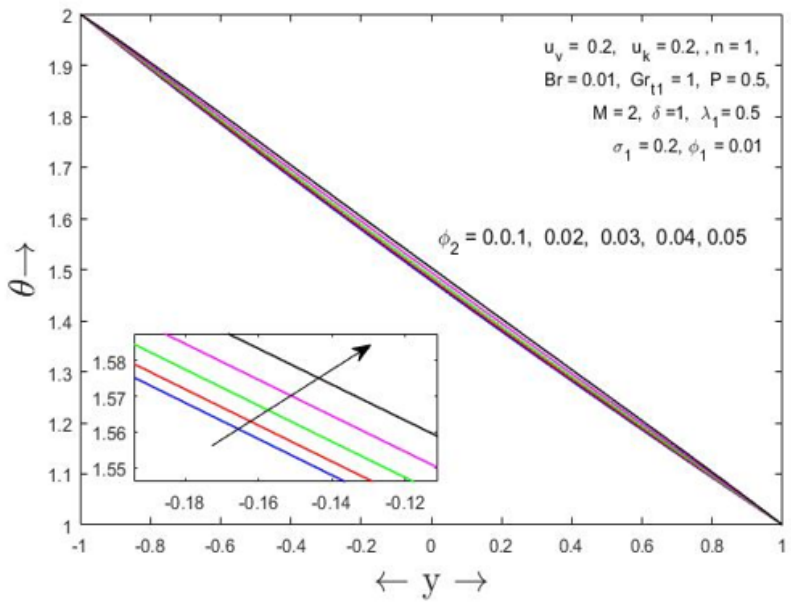

Figure 20: Temperature profiles for various values of ϕ_2

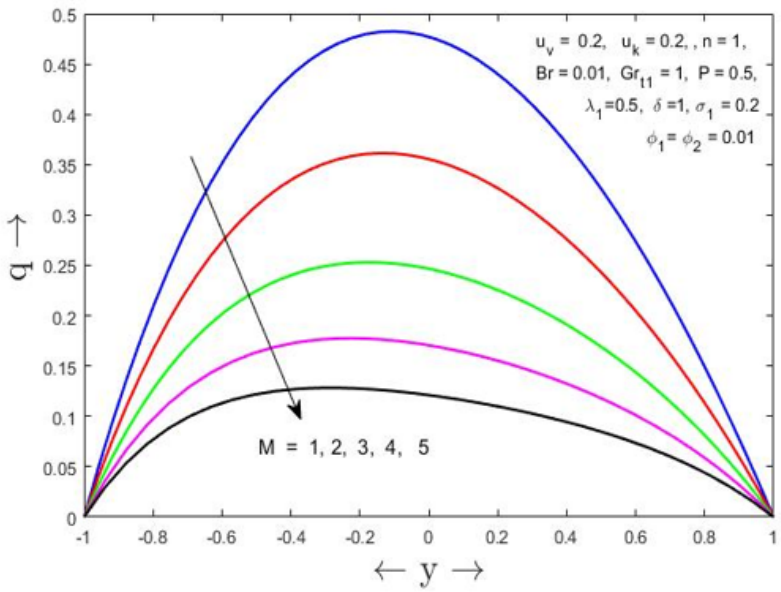

Figure 21: velocity profiles for various values of M

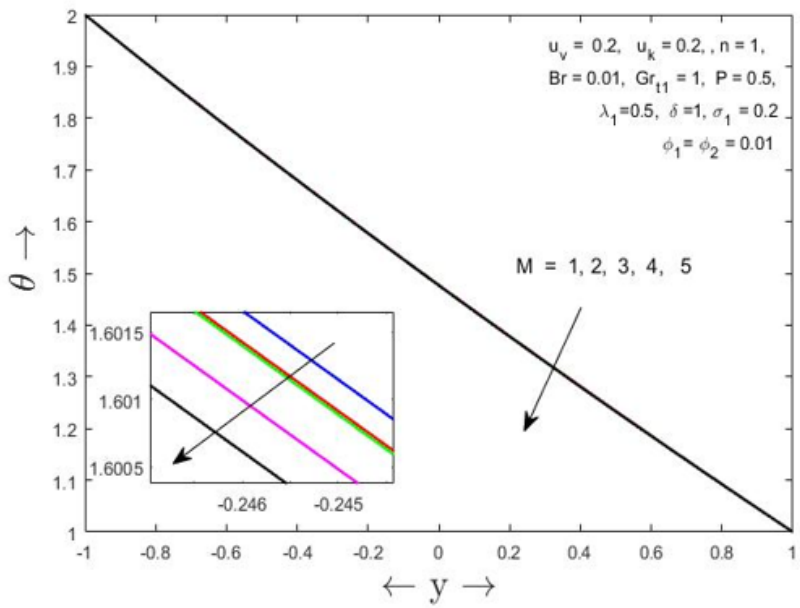

Figure 22: Temperature profiles for various values of M

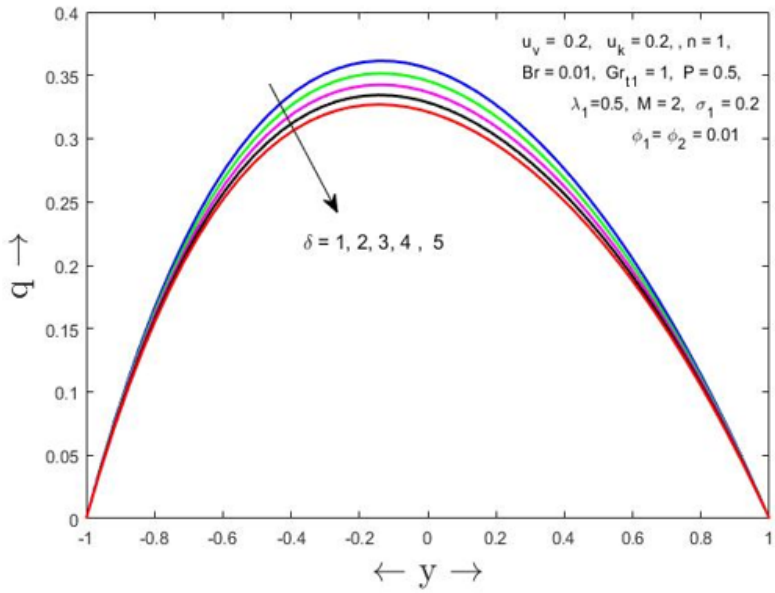

Figure 23: velocity profiles for various values of δ

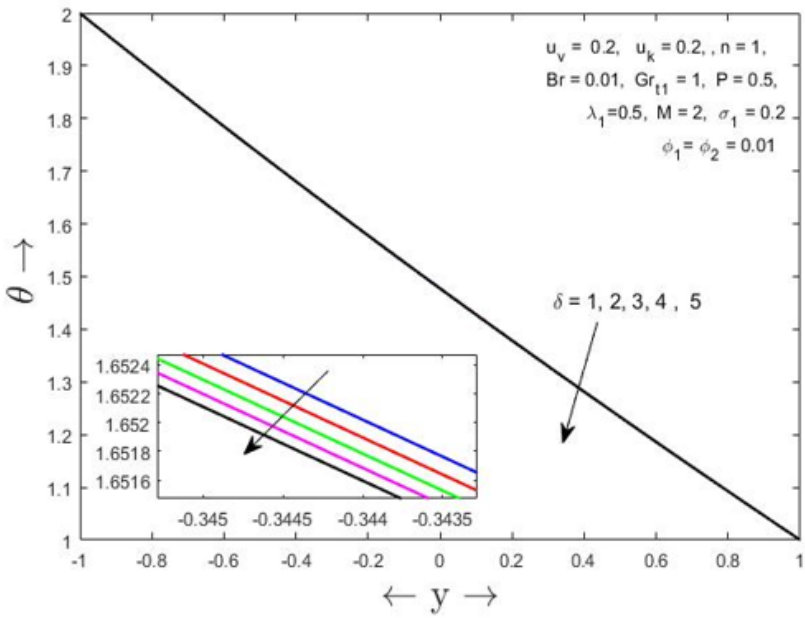

Figure 24: Temperature profiles for various values of δ

5. Skin Friction and Nusselt Number Analysis

Table 2: Effect of Governing Parameters on Skin Friction and Nusselt Number. Variable Viscosity u_v: Skin friction decreases as u_v increases because higher viscosity enhances internal resistance, reducing velocity gradients and wall shear. The Nusselt number increases slightly as viscous dissipation raises local temperature and thermal energy near the wall. Variable Thermal Conductivity u_k: Skin friction decreases while the Nusselt number increases significantly with u_v. Enhanced conductivity promotes heat

diffusion and reduces buoyancy induced velocity, lowering shear but strengthening temperature gradients and heat transfer. Thermal GrashofNumber Gr_{t_1}: Both skin friction and the Nusselt number increase with Gr_{t_1} because stronger buoyancy forces accelerate the flow enhance velocity gradients and intensify convective heat transfer.

Table 2: Computations showing the effect of governing parameters on skin friction and Nusselt numbers

	τ_1	τ_2	Nu_1	Nu_2
u_v	$u_k=-0.2,\ Gr_{t_1}=1,\ Br=0.01,\ P=0.5,\ n=1,\ \delta=1$ $\lambda_1=0.5,\ \sigma_1=0.2, \phi_1=0.01,\ \phi_2=0.01,\ M=2$			
-0.5	0.2178	-0.3071	0.2719	0.4431
-0.2	0.7024	-0.4893	0.2708	0.4443
0	0.7423	-0.5273	0.2702	0.4452
0.2	0.6852	-0.5254	0.2699	0.4457
0.5	0.5360	-0.4804	0.2712	0.4449
u_k	$u_v=0.2,\ Gr_{t_1}=1,\ Br=0.01,\ P=0.5,\ n=1,\ \delta=1$ $\lambda_1=0.5,\ \sigma_1=0.2, \phi_1=0.01,\ \phi_2=0.01,\ M=2$			
-0.5	0.6942	-0.5364	0.1925	0.3252
-0.2	0.6852	-0.5254	0.2699	0.4457
0	0.6789	-0.5183	0.4948	0.5044
0.2	0.6723	-0.5114	0.7648	0.5499
0.5	0.6622	-0.5014	1.2765	0.5989
Gr_{t_1}	$u_v=0.2,\ u_k=0.2,\ Br=0.01,\ P=0.5,\ n=1,\ \delta=1$ $\lambda_1=0.5,\ \sigma_1=0.2, \phi_1=0.01,\ \phi_2=0.01,\ M=2$			
1	0.6724	-0.5114	0.7647	0.5499
5	3.5987	-2.8452	0.4945	0.7161
10	7.2358	-5.7884	-0.3225	1.2243
15	11.288	-9.2305	-1.8465	2.2086
Br	$u_v=0.2,\ u_k=0.2,\ Gr_{t_1}=1,\ P=0.5,\ n=1,\ \delta=1$ $\lambda_1=0.5,\ \sigma_1=0.2, \phi_1=0.01,\ \phi_2=0.01,\ M=2$			
0.1	0.6865	-0.4733	1.1706	0.6433
0.5	0.7070	-0.49091	0.6789	0.8508
1	0.7379	-0.5176	-0.0522	1.1658
1.5	0.7746	-0.5499	-0.9253	1.5521
2	0.8172	-0.5880	-1.9567	2.0230
σ_1	$u_v=0.2,\ u_k=0.2,\ Gr_{t_1}=1,\ Br=0.01,\ P=0.5,\ n=1,$ $\delta=1,\ \lambda_1=0.5,\ \phi_1=0.01,\ \phi_2=0.01,\ M=2$			
0.5	0.6646	-0.5037	0.7649	0.5498
1	0.6389	-0.4783	0.7653	0.5495
2	0.5581	-0.4001	0.7666	0.5487
4	0.3969	-0.2547	0.7696	0.5468
ϕ_1	$u_v=0.2,\ u_k=0.2,\ Gr_{t_1}=1,\ Br=0.01,\ P=0.5,\ n=1,$ $\delta=1,\ \lambda_1=0.5,\ \sigma_1=0.2,\ \phi_2=0.01,\ M=2$			
0.01	0.6724	-0.5114	0.7648	0.5497
0.02	0.7189	-0.5494	0.7629	0.5510
0.03	0.7626	-0.5849	0.7609	0.5522
0.04	0.8034	-0.6182	0.7589	0.5534
0.05	0.8415	-0.6493	0.7568	0.5547
ϕ_2	$u_v=0.2,\ u_k=0.2,\ Gr_{t_1}=1,\ Br=0.01,\ P=0.5,\ n=1,$ $\delta=1,\ \lambda_1=0.5,\ \sigma_1=0.2, \phi_1=0.01,\ M=2$			
0.01	0.6724	-0.5114	0.7657	0.5497
0.02	0.9966	-0.7711	0.7471	0.5605
0.03	1.2981	-1.0119	0.7191	0.5774
0.04	1.5785	-1.2355	0.6805	0.6004
0.05	1.8398	-1.4437	0.6318	0.6295
δ	$u_v=0.2,\ u_k=0.2,\ Gr_{t_1}=1,\ Br=0.01,\ P=0.5,\ n=1,$ $M=2,\ \lambda_1=0.5,\ \sigma_1=0.2, \phi_1=0.01,\ \phi_2=0.01,$			
1	0.6724	-0.5115	0.7643	0.5503
2	0.6614	-0.5013	0.7647	0.5500
3	0.6515	-0.4922	0.7651	0.5497
4	0.6424	-0.4839	0.7656	0.5495
5	0.6342	-0.4762	0.7659	0.5493
λ_1	$u_v=0.2,\ u_k=0.2,\ Gr_{t_1}=1,\ Br=0.01,\ P=0.5,\ n=1,$ $\delta=0.1,\ \sigma_1=0.2, \phi_1=0.01,\ \phi_2=0.01,\ M=2$			
0.5	0.6724	-0.5114	0.7648	0.5497
1	0.8968	-0.6585	0.7586	0.5533
1.5	1.0130	-0.7302	0.7552	0.5551
2	1.0847	-0.7731	0.7531	0.5562
2.5	1.1335	-0.8018	0.7516	0.5569

Brinkman Number Br: Higher increases both skin friction and Nusselt number. Viscous dissipation converts kinetic energy into heat, raising temperature, viscosity and convective strength. Porous Param-

eter σ_1 : Increasing reduces skin friction by introducing drag resistance that suppresses velocity. Nusselt number changes only slightly, indicating that conduction still dominates heat transfer. Nanoparticle Volume Fractions ϕ_1, ϕ_2 : Increasing and raises both skin friction and Nusselt number. Nanoparticles enhance viscosity (raising wall shear) and thermal conductivity (enhancing heat transfer). Inertia Parameter δ : Skin friction decreases slightly with increasing delta as higher inertia enhances momentum relative to viscous forces. Nusselt number remains nearly constant, indicating conduction convection balance dominates heat transfer. Casson Parameter λ_1 : Skin friction increases as increases because higher yield stress elevates wall shear. Nusselt number also rises slightly due to increased viscous dissipation.

6. Comparison of Numerical Solutions for Velocity and Temperature

The present velocity and temperature results show excellent agreement with reference data [35] confirming the accuracy and reliability of the numerical scheme. Velocity profiles start at zero at the walls and reach a maximum at the channel centerline reflecting a classical parabolic velocity distribution characteristic of laminar flow. Temperature decreases monotonically from the hot wall to the cold wall, indicating effective thermal diffusion and convective heat transport. This validation strengthens the credibility of the model and numerical method used.

Table 3: Comparison results in velocity and temperature of $b_v = 0.2$, $b_k = 0.2$, $Gr_{t_1} = 1$,P =0.5,n = -1, $\lambda_1 = 0.5$, $\sigma = 0.2$,$\phi_1 = \phi_2 = 0.01$

$Br = 0$				
y	Umavathi et al. [35] $Gr_T = Gr_c = \sigma = 0$		Present work $\phi = \sigma = 0,\ Gr_{t_1} = 1$	
	Velocity	Temperature	Velocity	Temperature
-1.0	0.0000	2.0000	0.0000	2.0000
-0.8	0.0173	1.8743	0.0173	1.8743
-0.6	0.0268	1.7560	0.0268	1.7560
-0.4	0.0307	1.6444	0.0307	1.6444
-0.2	0.0310	1.5386	0.0310	1.5386
0.0	0.0287	1.4381	0.0287	1.4381
0.2	0.0246	1.3425	0.0246	1.3425
0.4	0.0193	1.2512	0.0193	1.2512
0.6	0.0133	1.1639	0.0133	1.1639
0.8	0.0068	1.0803	0.0068	1.0803
1.0	0.0000	1.0000	0.0000	1.0000

Table 3.1: Comparison results in velocity and temperature of $b_v = 0.2$, $b_k = 0.2$, $Gr_{t_1} = 1$,P =0.5,n = -1, $\lambda_1 = 0.5$, $\sigma = 0.2$,$\phi_1 = \phi_2 = 0.01$

$Br = 0.01$				
y	Umavathi et al. [35] $Gr_T = Gr_c = \sigma = 0$		Present work $\phi = \sigma = 0,\ Gr_{t_1} = 1$	
	Velocity	Temperature	Velocity	Temperature
-1.0	0.0000	0.0000	0.0000	2.0000
-0.8	0.0173	1.8762	0.0174	1.8762
-0.6	0.0268	1.7591	0.0268	1.7591
-0.4	0.0307	1.6480	0.0307	1.6480
-0.2	0.0310	1.5424	0.0310	1.5424
0.0	0.0287	1.4418	0.0287	1.4418
0.2	0.0246	1.3457	0.0246	1.3457
0.4	0.0193	1.2538	0.0193	1.2538
0.6	0.0133	1.1657	0.0133	1.1657
0.8	0.0068	1.0812	0.0068	1.0812
1.0	0.0000	1.0000	0.0000	1.0000

7. Conclusion

- Comprehensive modeling innovation : This study presents a rigorous numerical investigation of Casson hybrid nanofluid convection in a vertical porous channel with variable viscosity and thermal conductivity an integrated configuration seldom addressed simultaneously in prior literature.

- Realistic biomedical representation: By excluding electric field effects and emphasizing porous resistance, the model replicates physiologically relevant conditions, improving its applicability to blood flow, hyperthermia and targeted drug delivery environments.

- Critical role of variable properties: The inclusion of temperature dependent viscosity and thermal conductivity demonstrates their decisive influence on velocity suppression, boundary layer development and thermo regulatory enhancement of heat transport.

- Porous medium impact quantified: The model successfully isolates and quantifies the impact of porous resistance on momentum and energy transfer revealing pronounced velocity attenuation and boundary layer modulation essential for tissue engineering and perfusion based therapies.

- Enhanced convective performance: The present hybrid Casson model exhibits a 38.7% increase in average Nusselt number relative to our previous viscous fluid formulation highlighting the significant improvement in heat transfer efficiency. This enhancement aligns closely with recent experimental findings by [40] who reported comparable Nusselt number growth within similar parametric regimes.

- Parametric insights for control: Systematic variation of dimensionless parameters including Brinkman, Hartmann, Casson and Grashof numbers, wall temperature ratio and inertia reveals their coupled influence in modulating skin friction, flow acceleration and Nusselt number behavior.

- Non-Newtonian rheology significance: Casson rheology markedly reduces yield stress and alters viscosity momentum coupling, thereby promoting enhanced flow acceleration and improved thermal retention an essential feature for blood based bio fluid systems.

- Nanoparticle synergy validated: The synergistic combination of dual nanoparticles effectively boosts both thermal conductivity and momentum diffusion, augmenting convective performance while maintaining rheological stability compared with single nanoparticle suspensions.

- Model accuracy and credibility: Excellent agreement between computed velocity and temperature profiles with benchmark datasets validates the numerical framework, underscoring the robustness and reliability of the proposed formulation.

- Biomedical and engineering relevance: The findings provide a validated theoretical foundation for the design of advanced biomedical cooling devices, cancer hyperthermia systems, and perfusion-based therapeutic solutions, while also contributing fundamental insights to porous media transport and hybrid nanofluid dynamics.

References

1. Choi, S. U., Eastman, J., A., *Enhancing thermal conductivity of fluids with nanoparticles*, Argonne National Lab. (ANL), Argonne, IL (United States) (1995).
2. Acharya, N., Mabood, F., Shahzad, S., A., Badruddin, I., A., *Hydrothermal variations of radiative nanofluid flow by the influence of nanoparticles diameter and nanolayer*, Int Commun. Heat Mass Transf 130, 105781 (2022).
3. Krishnan, B., C., Rittgers, S., E., Yoganathan, A., P., *Biofluid Mechanics*: The Human Circulation, Taylor and Francis, New York, USA (2012). https://doi.org/10.1201/b11709
4. Tripathi, D., *Casson fluid model of blood flow in artery with magnetic field*, Journal of Applied Mathematics and Physics, 3(5), 621–630 (2015).
5. Blair, G., W., S., *An equation for the flow of blood, plasma and serum through glass capillaries*, Nature, 183, 613–614 (1959).
6. Copley, A., L., *Apparent viscosity and wall adherence of blood systems in Flow Properties of Blood and Other Biological Systems*, Eds. Pergamon Press, Oxford, UK (1960).
7. Ellahi, R., Rahman, S., U., Nadeem, S., Akbar, N., S., *Blood flow of nanofluid through an artery with composite stenosis and permeable walls.* Appl. Nanosci, 19–926 (2014). https://doi: 10.1007/s13204-013-0253-6
8. Syed, M., R., S., N, Muhammad,S.,N., Mir Asma, T., *Hydromagnetic flow of Casson nanofluid over a porous stretching cylinder with Newtonian heat and mass conditions*, Physica A: Statistical Mechanics and its Applications, 550 (2020). https://doi.org/10.1016/j.physa.2019.123988.
9. Imran, U., Sharidan, Sh., Makinde, O., D., Khan, I., *Unsteady MHD Falkner-Skan flow of Casson nanofluid with generative/destructive chemical reaction*, Chemical Engineering Science, 172, 694-706 (2017). https://doi.org/10.1016/j.ces.2017.07.011.
10. Ramesh, G., K., Gireesha, B., J., Shehzad, S., Abbasi, F., *Analysis of heat transfer phenomenon in magnetohydrodynamic casson fluid flow through Cattaneo – Christov heat diffusion theory*, Commun.Theor.Phys, 68, 1 (2017). https://dx.doi.org/10.1088/0253-6102/68/1/91.
11. Kumar, P., K., Paramasivam, P., Wanatasanappan, V., Dhanasekaran, S., Sharma, P., et. al. *Experimental and explainable machine learning approach on thermal conductivity and viscosity of water-based graphene oxide based mono and hybrid nanofluids.* Scientific Reports, 14, 30967 (2024). https://doi.org/10.1038/s41598-024-81955-1
12. Zaikovsky, A., V., Dmitrachkov, A., M., Morozova, M., A., *Thermal conductivity, viscosity and optical properties of nanofluids based on water and carbon nanoparticles*, Thermophysics and Aeromechanics, 31, 781–790 (2025). https://doi.org/10.1134/S0869864324040164
13. Anesu, N., Eanna, MC., C., Mayur, M., Saeid, H., Anouk, P., Mercedes, V., Dermot, B., *A review of physical, chemical and biological synthesis methods of bimetallic nanoparticles and applications in sensing, water treatment, biomedicine, catalysis and hydrogen storage*, Advances in Colloid and Interface Science, 321 (2023). https://doi.org/10.1016/j.cis.2023.103010.
14. Idris, D., S., Roy, A., *Synthesis of Bimetallic Nanoparticles and Applications An Updated Review*,Crystals, 13(4), 637 (2023). https://doi.org/10.3390/cryst13040637.
15. Pramod, K., Y., Aditya, S., *Biomedical simulations of electroosmotic non-Newtonian hybrid nanofluid (blood) with hematocrit viscosity through a porous overlapping irregular stenosed artery*, Computers in Biology and Medicine, 196, (part B) (2025). https://doi.org/10.1016/j.compbiomed.2025.110575.
16. Khalil, S., Yasmin, H., Abbas, T., Muhammad, T., *Analysis of thermal conductivity variation in magneto-hybrid nanofluids flow through porous medium with variable viscosity and slip boundary*, Case Studies in Thermal Engineering, 57, 104314 (2024). https://doi.org/10.1016/j.csite.2024.104314.
17. Bagai, S., Nishad, C., *Effect of temperature-dependent viscosity on natural convective boundary layer flow over a horizontal plate embedded in a nanofluid saturated porous medium, in: 5th International Conference* on Porous Media and Their Applications in Science, Engineering and Industry (2014).
18. Samal, S., Surender, O., *A model-based study on heat transfer and irreversibility in squeezing bio convectiv Casson hybrid nanofluid with variable conductivity: Sensitivity analysis*, Chinese Journal of Physics (2025). https://doi.org/10.1016/j.cjph.2025.03.023.
19. Mohammad, A., D., Bahram, J., Amir Mohammad, M., Payam, J., Ganji, D., *The effects of thermal radiation, thermal conductivity and variable viscosity on ferrofluid in porous medium under magnetic field.* World Journal of Engineering, 22, 1 (2023). https://doi.org/10.1108/WJE-09-2023-0402

20. Hamidreza, S., C., Saeed, D., *TiO_2-Ag/blood hybrid nanofluid flow through an artery with applications of drug delivery and blood circulation in the respiratory system*, International Journal of Numerical Methods for Heat Fluid Flow, 30, 11 (2020). https://doi.org/10.1108/HFF-10-2019-0732.

21. Praveen Kumar, V., Kanti, W., Vicki, N., Suman Saini, M., Vijayalaxmi, M., Prabhu Paramasivam, P., Yusuf, Md., *Thermal performance, entropy generation and machine learning insights of Al_2O_3–TiO_2 hybrid nanofluids in turbulent flow* Scientific Reports, 15 (2025). https://doi.org/10.1038/s41598-025-93749-0

22. Alharbi, S., O., Khalifa, H., A., EW., T., Gul, T., Alharbi, R., Alburaikan, A., Abdul, B., *The use of neural computational analysis for drug delivery applications results in hybrid nanofluid flow between the uniform gap of two concentric tubes*, Discov Appl Sci , 6, 4 (2024). https://doi.org/10.1007/s42452-024-05742-3.

23. Al-Bossly, A., *Modeling and Analysis of Blood-Based Hybrid Nanofluid Flow Containing Ag and TiO_2 Nanoparticles for Biomedical Applications*, A Non-Fourier Approach, BioNanoSci, 15 (2025). https://doi.org/10.1007/s12668-025-01865-y.

24. Alqarni, M., M., MahmoudE., E., Aljohani, M., A., *Dynamics of time-dependent Ag and TiO_2/blood Casson hybrid nanofluid squeezing flow past a Riga plate subject to an artificial neural network approach*, an application to drug delivery, Mech Time-Depend Mater, 29 (2025). https://doi.org/10.1007/s11043-025-09785-w

25. Mehrab, P., Rajabzadeh-Khosroshahi, M., Mohammad, M.,E., Erfan, R., Hamidreza, M., Rabia, A., R. AbbasR., Pandey, S., *TiO_2-based nanocomposites for cancer diagnosis and therapy: A comprehensive review*, Journal of Drug Delivery Science and Technology, 82 (2023). https://doi.org/10.1016/j.jddst.2023.104370

26. Anwar Saee, NiqabKhan, TazaGul, Wiyada Kumam, Wajdi Alghamdi, Poom Kumam., *The Flow of Blood-Based Hybrid Nanofluids with Couple Stresses by the Convergent and Divergent Channel for the Applications of Drug Delivery*, Molecules, 26(21), 6330 (2021). https://doi.org/10.3390/molecules26216330.

27. Sun, T., Zhang, Y., *The role of TiO_2 nanoparticles in drug delivery systems: From cytotoxicity to clinical applications.* Biomaterials, 276, 120917 (2021).

28. Sheikholeslami, M., Mousavi, S., M., *Numerical simulation of heat pipe solar system combined with finned thermal storage unit incorporating mixture of nanoparticles and paraffin*, International Communications in Heat and Mass Transfe, 155, 107468 (2024). https://doi.org/10.1016/j.icheatmasstransfer.2024.107468.

29. Chen, J., Sheng, D., Liu, L., Maitz, M., F., Liao, Y., Cui, J., Zhao, A., Yang, P., Huang, N., Wang,Y., Photofunctionalized TiO_2 nanotubes decorated with multifunction Ag nanoparticles for enhanced vascular biocompatibility, Bioactive Materials, 6(1), 45-54 (2021). https://doi.org/10.1016/j.bioactmat.2020.07.009.

30. Nazar, T., Bhatti, M., M., Michaelides, E., E., *Hybrid (Au-TiO_2) nanofluid flow over a thin needle with magnetic field and thermal radiation: Dual solutions and stability analysis Microfluid*, Nanofluidics , 26 (2021).

31. Chahregh, H., S., Dinarvand, S., *TiO_2-Ag/blood hybrid nanofluid flow through an artery with applications of drug delivery and blood circulation in the respiratory system*, International Journal of Numerical Methods for Heat Fluid Flow, Emerald Publishing Limited 0961-5539 (2019). https:// doi.org/10.1108/HFF-10-2019-0732.

32. Algehyne, E., A., Ameer Ahammad, N., E. Elnair, Mohamed Zidan Yasir, Y. Alhusayni, B.O.El-Bashir, Anwar Saeed, Ali Saleh Alshomrani, Faris Alzahrani, *Enhancing Heat Transfer in Blood Hybrid Nanofluid Flow with Ag–TiO_2 Nanoparticles and Electrical Field in a Tilted Cylindrical W-Shape Stenosis., Artery*, A Finite Difference Approach Symmetry 15, 1242 (2023). https://doi.org/10.3390/sym15061242.

33. Umavathi, J., C., Sheremet, M., A., Mohiuddin, S., *Combined effect of variable viscosity and thermal conductivity on mixed convection flow of a viscous fluid in a vertical channel in the presence of first order chemical reaction*, Eur. J. Mech. B/Fluids, 58, 98–108 (2016).

34. Umavathi, J., C., Shekar, M., *Combined effect of variable viscosity and thermal conductivity on free convection flow of a viscous fluid in a vertical channel using DTM*, Meccanica, 51, 71–86 (2016).

35. Umavathi, J., C., Syed Mohiuddin, *Mixed convection flow of permeable fluid in a vertical channel in the presence of first-order chemical reaction: Variable Properties*, Special Topics Reviews in Porous Media-An International Journal, 9(2), 155–176 (2018). http://dx.doi.org/10.1615/SpecialTopicsRevPorousMedia.v9.i2.50

36. Annapurna, T., Sridhar, K., S., R., Karuna Prasad, M., *Effect of Different Shapes of Nanoparticles on Mixed Convective Nanofluid Flow in a Darcy-Forchhiemer Porous Medium*, CFD Letters, 16, 38-58 (2024). https://doi.org/10.37934/cfdl.16.12.3858

37. EbrahemAlgehyne, A., Ameer Ahammad, N., Elnair, Md.,E., Zidan, Md., Yasir, Alhusayni, Y., Babikir, Y., Osman El-Bashir, Anwar Saeed, Ali Saleh Alshomrani , Faris Alzahrani, *Enhancing Heat Transfer in Blood Hybrid Nanofluid Flow with Ag- TiO_2 Nanoparticles and Electrical Field in a Tilted Cylindrical W-Shape Stenosis Artery*, A Finite Difference Approach, 15(6), 1242 (2023). https://doi.org/10.3390/sym 15061242

38. Elie Nader, Sarah Skinner, Marc Romana, Romain Fort, Nathalie Lemonne, Nicolas Guillot, Alexandra Gauthier, Sophie Antoine-Jonville, Céline Renoux, Marie-Dominique Hardy-Dessources, Emeric Stauffer, Philippe Joly, Yves Bertr and Philippe Connes *Blood Rheology: Key Parameters, Impact on Blood Flow, Role in Sickle Cell Disease and Effects of Exercise* frontiers in Physiology amphibian and reptile science, 1329 (2019). https://doi.org 10.3389/fphys.2019.01329

39. Attia, H.,A., *Unsteady hydromagnetic channel flow of dusty fluid with temperature dependent viscosity and thermal conductivity*, J.Heat Mass Transf, 42, 779–787 (2006).

40. Khadanga, V., PurnaChandra, Mishra, Sayantan Mukherjee, Naser Ali, *Experimental evaluation and artificial neural network modeling of heat transfer performance of aerosolized magnesium oxide nanoparticles flow through pipe*, Chinese Journal of Physics 1217-1232 (2024). https://doi.org/10.1016/j.cjph.2024

Nomenclature

Physical symbols

q_1	velocity (m s^{-1})
q	dimensionless fluid velocity
$\bar{q}$	mean velocity (m s^{-1})
Y	coordinate axis (m)
y	dimensionless coordinate axis
T_0	reference temperature (K)
T	fluid temperature (K)
T_1, T_2	wall temperatures (K)
g	acceleration due to gravity (m s^{-2})
k	thermal conductivity of the fluid (W m^{-1} K^{-1})
u_{v1}	viscosity variation parameter
u_k	thermal conductivity at temperature T_0 (W m^{-1} K^{-1})
n	wall temperature ratio
b	channel width
B_0	conductivity variation parameter
c_f	intertial (Forchheimer) coefficient

Dimensionless Symbols

Br	Brinkman number
M	Hartmann number
Gr	Grashof number
Gr_{t_1}	thermal Grashof number
Re	Reynolds number
δ	Forchheimer number

Greek letters

λ_1	Casson parameter
λ_{T_1}	coefficient of thermal expansion (K^{-1})
θ	dimensionless temperature
μ	dynamic viscosity (kg m^{-1} s^{-1})
μ_0	dynamic viscosity at temperature T_0 (kg m^{-1} s^{-1})
ρ	density of the fluid (kg m^{-3})
ρ_0	static density
φ	rescaled species concentration
τ_1, τ_2	skin friction
ΔT	difference in temperature
σ_1	porous parameter (m^{-2})
κ_1	permeability of the porous medium

Suffix

f	quantities for base nanofluid
s	solid particles
hnf	hybrid nanofluid
n	nanofluid
s	solid particle
f	base fluid (blood)
T	thermal
0	reference state
$1, 2$	surface conditions

Annapurna Tarapuram,
Department of Mathematics,
Ballari Institute of Technology and Management,
Ballari–583104, India.
Affiliated to Visvesvaraya Technological University,
Belagavi–590018, India.
E-mail address: annapurna.t9@gmail.com

and

*Syed Mohiuddin**,
Department of Mathematics,
Ballari Institute of Technology and Management,
Ballari–583104, India.
E-mail address: simoh14@gmail.com

and

M. Karuna Prasad,
Department of Mathematics,
Kishkinda University,
Ballari–583120, India.
E-mail address: karunaprasad9@gmail.com

and

Suneetha Kolasani,
Department of Mathematics,
Ballari Institute of Technology and Management,
Ballari–583104, India.
E-mail address: sunitha.kolasani@gmail.com